No Internal Connections Detected Between Leading Decadal to Multidecadal Climate Modes in North Atlantic and North Pacific Basins

Tyler M. Fenske[1] and Amy C Clement[1]

[1]University of Miami

November 21, 2022

Abstract

Previous studies have attempted to unravel possible connections between leading decadal to multidecadal climate modes in the North Atlantic and North Pacific ocean basins, the Atlantic Multidecadal Variability in the North Atlantic, and the Pacific Decadal Oscillation and Victoria Mode in the North Pacific. We use newly available climate model data and apply improvements to existing methods to rexamine relationships among the different modes. Our main tool is the Multi-Model Large Ensemble Archive, which includes 270 ensemble members and allows for isolation of the forced and internal components of climate variability. Our results suggest that any internal connections between these modes are indistinguishable from random noise. Further, external forcing is shown to affect each region in similar ways, suggesting that climate change could be an indirect link between the two basins, and can confound the interpretation of he relationship between the basins.

Geophysical Research Letters

Supporting Information for

No Internal Connections Detected Between Leading Decadal to Multidecadal Climate Modes in North Atlantic and North Pacific Basins

T. Fenske[1] and A. Clement[1]

[1]Rosenstiel School of Marine and Atmospheric Science, University of Miami, Miami, Florida

Contents of this file

Supplemental Table 1 Supplemental Figure 1 Supplemental Figure 2 Supplemental Figure 3

Additional Supporting Information (Files uploaded separately)

None

Modeling Center	CCCma	CESM	CSIRO	GFDL	GFDL	MPI
Model Version	CanESM2	CESM1-CAM5	MK3.6	CM3	ESM2M	MPI-ESM-L

Modeling Center	CCCma	CESM	CSIRO	GFDL	GFDL	MPI
Initialization Method	Macro/Micro	Micro	Macro	Micro	Macro	Macro
# of Ensemble Members	50	39	30	20	30	100
Latitude Resolution (grid points)	2.75° (64)	<1° (192)	1.85° (96)	2° (90)	2° (90)	1.875° (96)
Longitude Resolution (grid points)	2.8125° (128)	1.25° (288)	1.875° (192)	2.5° (144)	2.5° (144)	1.875° (192)
Start Year	1950	1920	1850	1920	1950	1850
PI Length	296 years	319 years	500 years	200 years	200 years	281 years

Table S1. Details of the six large ensembles from the MMLEA and observations used in this study, adapted from Deser et al. (2020) and from the MMLEA data webpage.

Hosted file

`image2.emf` available at https://authorea.com/users/529866/articles/597210-no-internal-connections-detected-between-leading-decadal-to-multidecadal-climate-modes-in-north-atlantic-and-north-pacific-basins

Supplemental Figure 1. Cross-correlation matrix of HADISST observed linearly-detrended filtered climate pattern time series. All possible cross-correlations between each of the three EOF modes in each basin are shown. From left to right: NA-EOF1, NA-EOF2, and NA-EOF3. From top to bottom: NP-EOF1, NP-EOF2, and NP-EOF3. Black lines represent statistical significance thresholds generated using the peak test, while green lines represent the cross-correlations for the corresponding modes. Lags correspond to the NA (NP) mode leading for positive (negative) lags.

Hosted file

`image3.emf` available at https://authorea.com/users/529866/articles/597210-no-internal-connections-detected-between-leading-decadal-to-multidecadal-climate-modes-in-north-atlantic-and-north-pacific-basins

Supplemental Figure 2. The effect linear detrending has on observed EOFs in the NP. For observations where no detrending occurs, A) and C) show the first EOF spatial pattern and time series respectively. B) and D) show the same but for the second EOF. For linearly detrended observations, E) and G) show the first EOF spatial pattern and time series respectively, while F) and H) show the same for the second EOF. I) shows the time series from C) (linearly detrended) and H) together to show their similarity (93% correlation, significant at the 99% threshold). The red curves are the same time series, while the blue curve in I) is equivalent to the time series in C) but with the linear slope removed.

Hosted file

`image4.emf` available at https://authorea.com/users/529866/articles/597210-no-internal-connections-detected-between-leading-decadal-to-multidecadal-climate-modes-in-north-atlantic-and-north-pacific-basins

Supplemental Figure 3. EOF spatial patterns. From top to bottom: HADISST (observations), CANESM2, CESM, CSIRO MK36, GFDL CM3, GFDL ESM2M, and MPI (six MMLEA models). From left to right: NA-EOF1, NP-EOF1, NP-EOF2, and NP-EOF3. MMLEA patterns are internal (full minus ensemble mean) composite means (EOF analysis is performed on each member, and then the resulting EOFs are averaged across all members). Color scale is dimensionless, following standard EOF output.

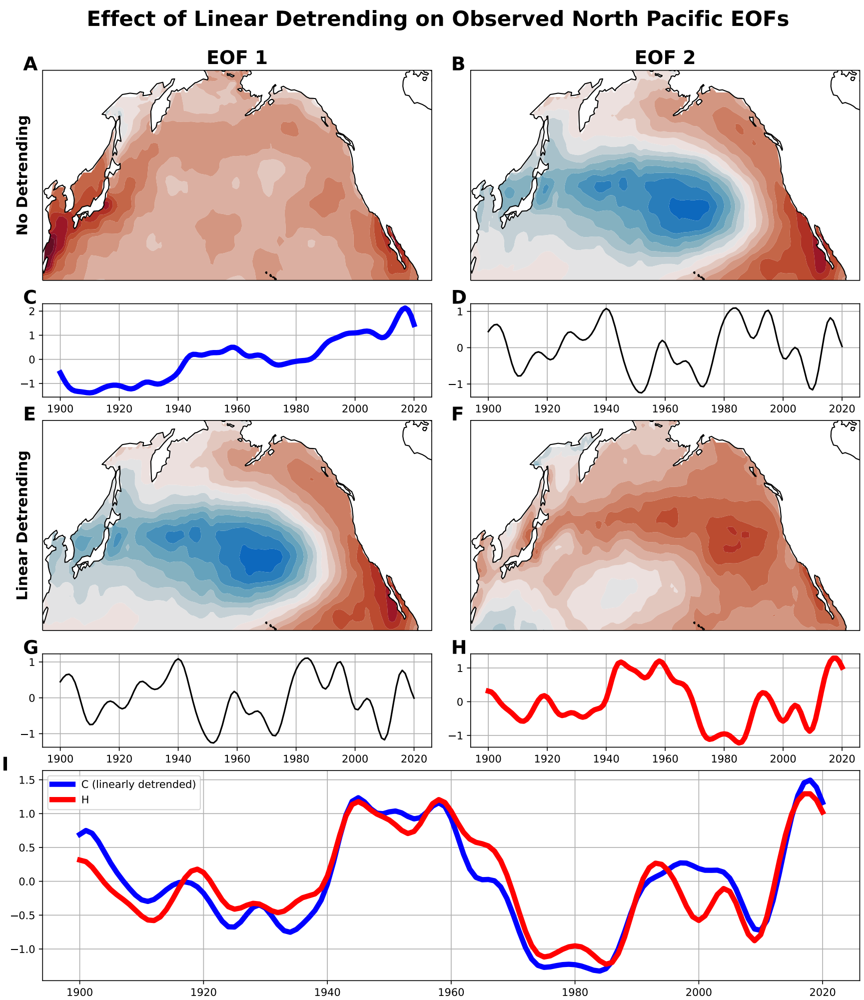
Effect of Linear Detrending on Observed North Pacific EOFs
EOF 1
EOF 2
No Detrending
Linear Detrending
C (linearly detrended)
H

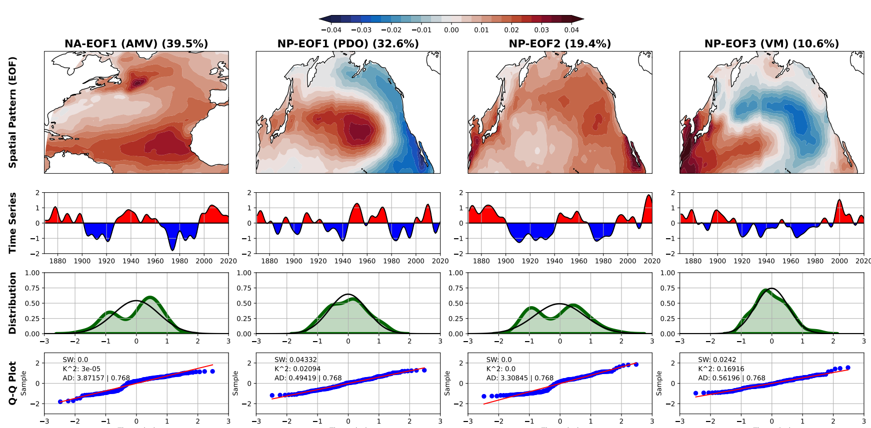
NA-EOF1 (AMV) (39.5%)
NP-EOF1 (PDO) (32.6%)
NP-EOF2 (19.4%)
NP-EOF3 (VM) (10.6%)
Spatial Pattern (EOF)
Time Series
Distribution
Q-Q Plot
Theoretical
Sample

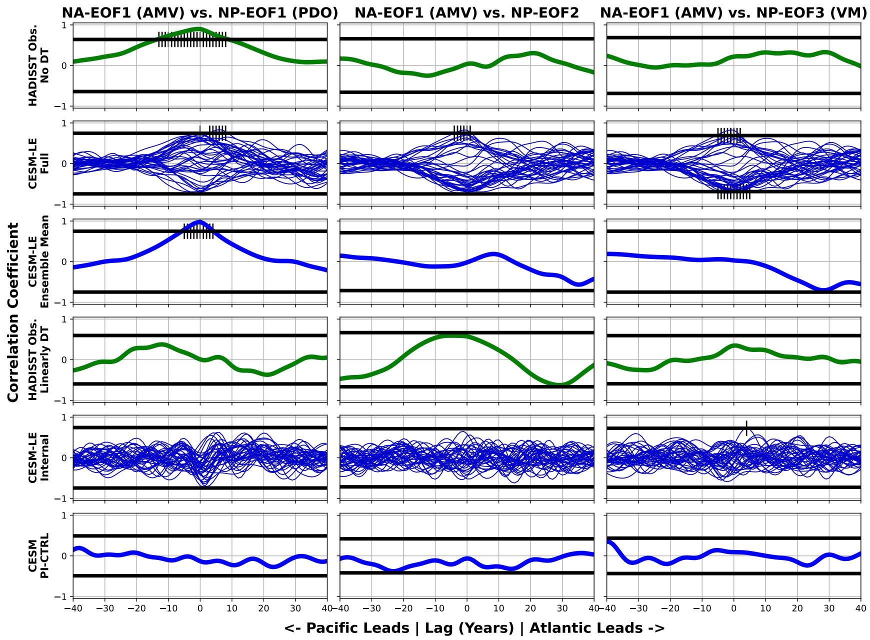

HADISST Observed (Linear Detrending) North Atlantic vs. North Pacific Cross Correlations

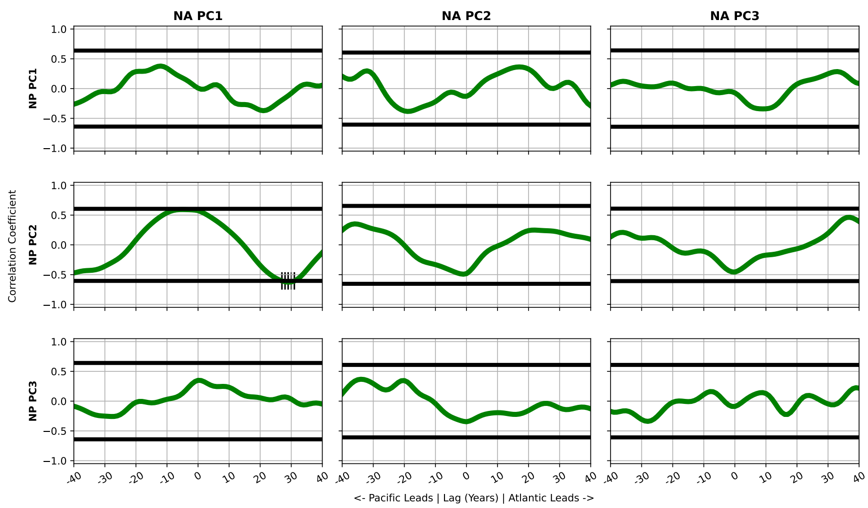

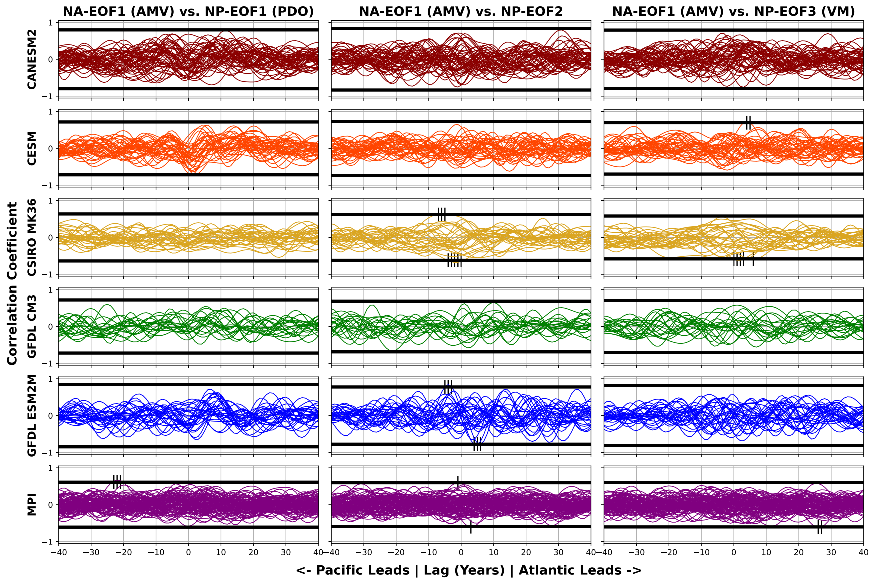
NA-EOF1 (AMV) vs. NP-EOF1 (PDO)
NA-EOF1 (AMV) vs. NP-EOF2
NA-EOF1 (AMV) vs. NP-EOF3 (VM)
CANESM2
CESM
CSIRO MK36
GFDL CM3
GFDL ESM2M
MPI
Correlation Coefficient
<- Pacific Leads | Lag (Years) | Atlantic Leads ->

No Internal Connections Detected Between Leading Decadal to Multidecadal Climate Modes in North Atlantic and North Pacific Basins

T. Fenske[1] and A. Clement[1]

[1]Rosenstiel School of Marine and Atmospheric Science, University of Miami, Miami, Florida

Corresponding author: Tyler Fenske (tyler.fenske@rsmas.miami.edu)

Key Points:

- Novel methods are applied to decadal to multidecadal climate modes to analyze possible relationships between modes in different basins.
- An analysis of relationships between leading North Atlantic and North Pacific climate modes does not reveal any internal connections, challenging previous results.
- External forcing such as global warming is shown to be a possible confounding factor in climate relationships.

Abstract

Previous studies have attempted to unravel possible connections between leading decadal to multidecadal climate modes in the North Atlantic and North Pacific ocean basins, the Atlantic Multidecadal Variability in the North Atlantic, and the Pacific Decadal Oscillation and Victoria Mode in the North Pacific. We use newly available climate model data and apply improvements to existing methods to rexamine relationships among the different modes. Our main tool is the Multi-Model Large Ensemble Archive, which includes 270 ensemble members and allows for isolation of the forced and internal components of climate variability. Our results suggest that any internal connections between these modes are indistinguishable from random noise. Further, external forcing is shown to affect each region in similar ways, suggesting that climate change could be an indirect link between the two basins, and can confound the interpretation of he relationship between the basins.

Plain Language Summary

We examine possible connections between climate patterns in the North Atlantic and North Pacific oceans. New climate model data and improved statistical methods allow us to build on previous research of these links. In contrast to previous studies, no natural connections are detected. However, global warming is shown to affect each region in similar ways, suggesting that climate change could be an indirect link between the two basins.

Introduction

Climate modes are considered to be the leading source of internal climate variability, affecting weather and climate patterns across the globe. These long-distance effects are sometimes referred to as teleconnections and are driven by atmospheric bridges (Alexander et al. 2002, Liu and Alexander 2007). Sea-surface temperature (SST) variability associated with a particular climate mode is coupled to the atmosphere, allowing the mode to change the overlying atmospheric circulation. This signal is then transported through the atmosphere to other regions, where the variability influences the ocean in a distant location, potentially imprinting on or even exciting a different climate mode there (e.g. Liu and Alexander 2007, Dommenget and Latif 2008). The magnitude of control a climate mode has on another region can also vary in time, adding another dimension to potential interactions and making them more difficult to identify (Raible et al. 2014). The possibility of climate mode interactions must be considered to fully understand the sources of internal climate variability.

Here, we focus on potential interactions between decadal to multidecadal climate modes in the North Atlantic (NA) and North Pacific (NP) ocean basins. In the NA, low-frequency variability is captured via the Atlantic Multidecadal Oscillation (AMO) or Atlantic Multidecadal Variability (AMV) (Enfield et al. 2001). In the NP, two modes are commonly used to capture the low-frequency variability. The Pacific Decadal Oscillation (Mantua et al. 1997) and the Victoria Mode (VM) (Bond et al. 2003) or North Pacific Gyre Oscillation (NPGO) (Di Lorenzo et al. 2008) are the two leading modes of decadal and multidecadal variability respectively. Many other methods of capturing variability in these basins have since been developed (Eden and Jung 2001, Salinger et al. 2001, Martin et al. 2019, Nigam et al. 2020, etc.), although convention has maintained scientific usage of the AMV and PDO as the dominant low-frequency modes.

Despite their extensive usage, these modes, especially the AMV, may not adequately isolate and capture a single source of internal variability (Marini and Frankignoul 2014; Wills et al. 2018; O'Reilly et al. 2019, etc.). Representing multidecadal variability with relatively short observed periods (order of 100 years) is also challenging, especially when low-pass filtering is applied (Cane et al. 2017). Assuming oscillatory variability, only one or two full cycles may be observed (Mann et al. 2021). This reduces the effective degrees of freedom and subsequently requires care to be taken during statistical analysis, especially regarding significance testing.

Several previous studies have worked on the NA-NP relationship, all of which suggest that the two basins have some statistical relationship with each other. Both d'Orgeville and Peltier (2007) and Zhang and Delworth (2007) relate the first two Empirical Orthogonal Functions or Principal Components (EOFs or PCs, hereafter referred to as EOFs) of NP SSTs to a metric for the AMV (d'Orgeville and Peltier use the first EOF of NA SSTs, while Zhang and Delworth use NA area mean SSTs), although they utilize those EOFs in different ways. d'Orgeville and Peltier combine them and then isolate the 20 year (analogous to the PDO) and 60 year (analogous to the VM) period wavelets and conclude that there is a singular source driving variability in each region, while Zhang and Delworth use the two EOFs and conclude that the Atlantic Meridional Overturning Current (AMOC) drives the AMV, which in turn drives the PDO/VM through atmospheric teleconnections. Wu et al. (2011) use the first two EOFs of each basin and finds a statistically significant link. Marini and Frankignoul (2014) use several methods attempting to deconstruct the origin of the AMV, such as dynamical filtering and removing trends in various manners. Their analysis includes a comparison of the AMV and PDO, where they come to a similar conclusion as previous studies. Nigam et al. (2020) uses global rotated empirical orthogonal functions (EOFs) to represent all major global modes, and their modes most similar to the AMV and PDO also support a relationship existing. An et al. (2021) use ensemble pacemaker experiments to suggest that multidecadal Pacific variability is generated by AMO forcing and local air-sea interactions. These studies use the student's t-test for significance thresholds, with Wu et al. (2011) also using customized bootstrap methods. All of these studies are in agreement that a modest but statistically significant correlation exists with the AMV leading the PDO by 12-14 years.

Here we will build upon those previous examples using a novel dataset, the Multi-Model Large Ensemble Archive (MMLEA), and improve on existing methods, such as significance testing and mode definitions. Using these tools, we reanalyze the potential relationships between low-frequency climate variability in the NA and NP ocean basins. Our results challenge previous findings, suggesting that a relationship is not statistically significant. We also focus on the role that external forcing plays in the inter-basin relationship and find that it may be a confounding factor.

Data

For SST observational data, we use the UK Met Office's Hadley Centre Sea Ice and SST data set (HADISST) (Rayner et al. 2003). Data is linearly detrended at each grid point, and we use 151 years of monthly data from 1870-2020. We repeat our analysis with other common SST datasets and find no qualitative differences.

Our primary tool is the new Multi-Model Large Ensemble Archive (MMLEA) (Deser et al. 2020). Necessary output is currently available for six ensembles included in the MMLEA (each hereafter as CANESM2, CESM, CSIRO-MK36, GFDL-CM3, GFDL-ESM2M, and MPI). Each ensemble contains at least 20 members for a total of 269 members (50, 39, 30, 20, 30, and 100 respetively). All MMLEA members are from the CMIP5 era and use historical forcing. Data from each member is cut off at the year 2020 to match the observed period. We also use each member's corresponding pre-industrial control run (PI), which are separate from the MMLEA. One advantage of large ensembles is their capability to extract the forced signal from each member by subtracting the ensemble mean (Kay et al. 2015). More details on the MMLEA are provided in Table S1 (adapted from Deser et al. 2020).

Mode Definitions

Our mode definitions for each basin loosely follow the conventions for the AMV, PDO, and VM (Enfield et al. 2001, Mantua et al. 1997, and Bond et al. 2003 respectively). Instead of applying unique methods (EOF analysis for the NP, regional area mean for the NA) to each basin, we apply EOF analysis to each basin in an attempt to better capture individual modes of variability. We compute the first three EOFs over the NP region of 20°N-65°N, 120°E-100°W and the first EOF over the NA region of 0°N-65°N, 120°W-0°. We also compute further EOFs for the NA, however these do not have as clear of a physical interpretation and do not affect our results in any meaningful way. They are not included except in Supplemental Figure 1, which shows a matrix of relationships between the first three EOFs of each basin, with no significant relationships involving any NA EOFs except the first. Figure 1 shows the spatial patterns of these EOF modes in the first row, while the second row shows the corresponding time series. NA-EOF1 represents the AMV, characterized by a tripole spatial pattern and a predominantly multi-decadal time series. NP-EOF1 represents the PDO, characterized by a dipole spatial pattern with warming (cooling) in the central NP and cooling (warming) along the eastern boundary, along with a mostly decadal time series. NP-EOF3 represents the VM, also characterized by a dipole pattern offset to the west from the PDO's, as well as a mostly decadal time series.

A major challenge in understanding climate mode drivers is separating internal variability from externally forced variability. This is typically achieved by removing the estimated forced trend. MMLEA data is detrended by removing the ensemble mean, following Deser et al. (2020). We define full variability (hereafter full) as the unmodified output of each member of the MMLEA, and we define internal variability as the full minus the ensemble mean. Observations are detrended linearly at each grid point, following convention. Figure 2 shows the effects of linear detrending on the EOF analysis in the NP. When no detrending occurs, the first EOF captures the externally forced global warming signal based on its uniform warming pattern, while the second EOF is clearly the PDO. Linear detrending causes the PDO to become the first EOF, while the second EOF still resembles the externally forced signal. Comparing the time series of these two apparent global warming signals reveals that they are remarkably similar. The second EOF of linearly detrended NP SSTs resembles the non-linear features of the global warming signal. Similar results exist for the NA (not shown). Other more complex detrending methods exist and offer different interpretations about what is forced versus what is internal, especially in the Atlantic (e.g. Frankignoul et al. 2017, Qin et al 2020). However, these differences in forced signals are not substantial enough to affect our results qualitatively.

Note that the composite mean and the ensemble mean are distinct and computed differently, namely in the order of operations because EOF analysis is a non-linear computation. Here, the composite mean is defined as EOF analysis being done first, followed by averaging of the EOFs. In contrast, the ensemble mean is where averaging is done first, and then EOF analysis is performed on the averaged SSTs. Physically, the ensemble mean represents the externally forced signal in each model, while the composite mean represents the average internal modes across all members.

All time series are normalized and smoothed with a 10-year low-pass Lanczos filter to focus on decadal to multi-decadal variability, following classical methods.

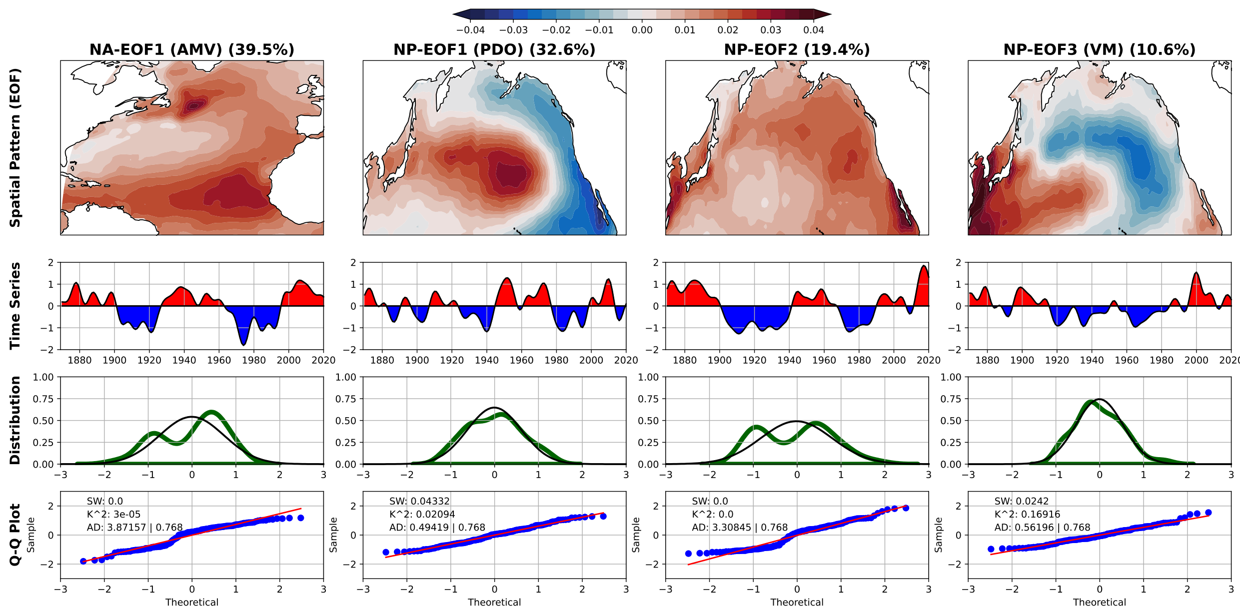

Figure 1. EOF modes and normality analysis of observed HadISST linearly-detrended North Atlantic and North Pacific SSTs. From left to right: NA-EOF1, NP-EOF1, NP-EOF2, and NP-EOF3. The percentage at the top of each column represents the variance explained by each EOF. NA-EOF1 is analogous to the AMV, NP-EOF1 to the PDO, and NP-EOF3 to the VM. NP-EOF2 is analogous to the non-linear global warming signal (more detail in text). Rows from top to bottom: 1) Spatial patterns of each EOF mode. Red (blue) corresponds to warming (cooling) when time series is positive (negative). 2) Filtered time series of each EOF mode. 3) Probability distribution of each time series are shown with shaded green curves; corresponding standard normal distributions are shown with black curves. 4) Quantile-quantile plots with data shown in blue points. A standard normal distribution is shown in red for comparison. Three quantitative assessments of normality are also applied: 1) The Shapiro-Wilk Test (SW). The corresponding p-value is listed, with p-values greater than 0.05 (95% confidence) implying a normal distribution. 2) D'Agostino's K-Squared Test (K^2). The corresponding p-value is listed, with p-values greater than 0.05 (95% confidence) implying a normal distribution. 3) The Anderson-Darling Test (AD). The first value is the resulting measure of normality, and the second value is the 95% critical value for the AD test. If the first value is smaller than the critical value, the distribution can be assumed to be normal. All tests should be considered equally in determining whether or not to assume a normal distribution.

Normality of Modes

To determine whether standard parametric statistics can be used or not, the normality of our time series must be assessed first. While non-Gaussian parametric statistics exist, Gaussian assumptions are common with geophysical time series analysis and are used by the previous studies on the NA-NP inter-basin relationships (d'Orgeville and Peltier, 2007, Zhang and Delworth 2007, Wu et al. 2011, Marini and Frankignoul 2014, and Nigam et al. 2020).

We test the four modes' filtered time series with five normality tests as recommended by Yap and Sim (2011) and Ghasemi and Zahediasl (2012). Two are qualitative assessments: a histogram with a standard normal curve fitted to the data (Figures 1I-L), and a quantile-quantile plot (Figures 1M-P). Three are quantitative: the Shapiro-Wilk test (SW), the D'Agostino skewness test (K^2), and the Anderson-Darling test (AD) (shown as text in Figures 1M-P). Only NP-EOF3 passes more than a single quantitative test. The combination of all tests generally suggests that only NP-EOF3 of the filtered time series can be described as normal, so Gaussian assumptions cannot be made for analysis of mode relationships. Therefore, non-parametric statistics are required for significance testing.

Significance Testing

We use a non-parametric bootstrapping method for significance testing. Our primary statistical tool is cross-correlation, so we build this method to evaluate the significance of a given "real" cross-correlation. We create sets of random white-noise time series by shuffling each observed unfiltered time series 1000 times. We also used sets of AR1 red noise (Katz 1982) and quantile-mapped sets (Maraun 2013) and found no qualitative differences in our results. Each random time series is filtered, and each possible pair of modes between each basin is cross-correlated for the entire random set. These 1000 cross-correlations are then used to compute 95% significance thresholds for the corresponding observed cross-correlation. This method is similar to the bootstrap used by Wu et al. (2011), although our method differs slightly. Wu et al. (2011) calculate the 95th percentile at each specific lag in their cross correlation (hereafter the "point test").

Their interest, however, is not on a particular lag, but instead of the peaks of the cross-correlation that are above the significance threshold. The specific lag at which these peaks occurred was unimportant - whether it occurred with 0 year lag or 30 years lag, their conclusions would remain the same. By definition, their statistical test requires that a particular lag be of interest, meaning that the lag at which the peaks occur *is* important, contrary to their conclusions. This can be viewed as an *a priori* test with an *a posteriori* conclusion, which suggests their significance thresholds may not be appropriate.

Alternatively, a "peak test" can be used. Instead of calculating the significance thresholds at each lag, we choose the maximum value of each random cross-correlation to compute the thresholds from. The result is that at 95% confidence, 5% of random cross-correlations have any points that are significant when using the peak test, while ~50% have significant points when using the point test. This shows that using an improper significance test can result in many spurious significant points on any given cross-correlation. All significance thresholds shown here are computed using the peak test.

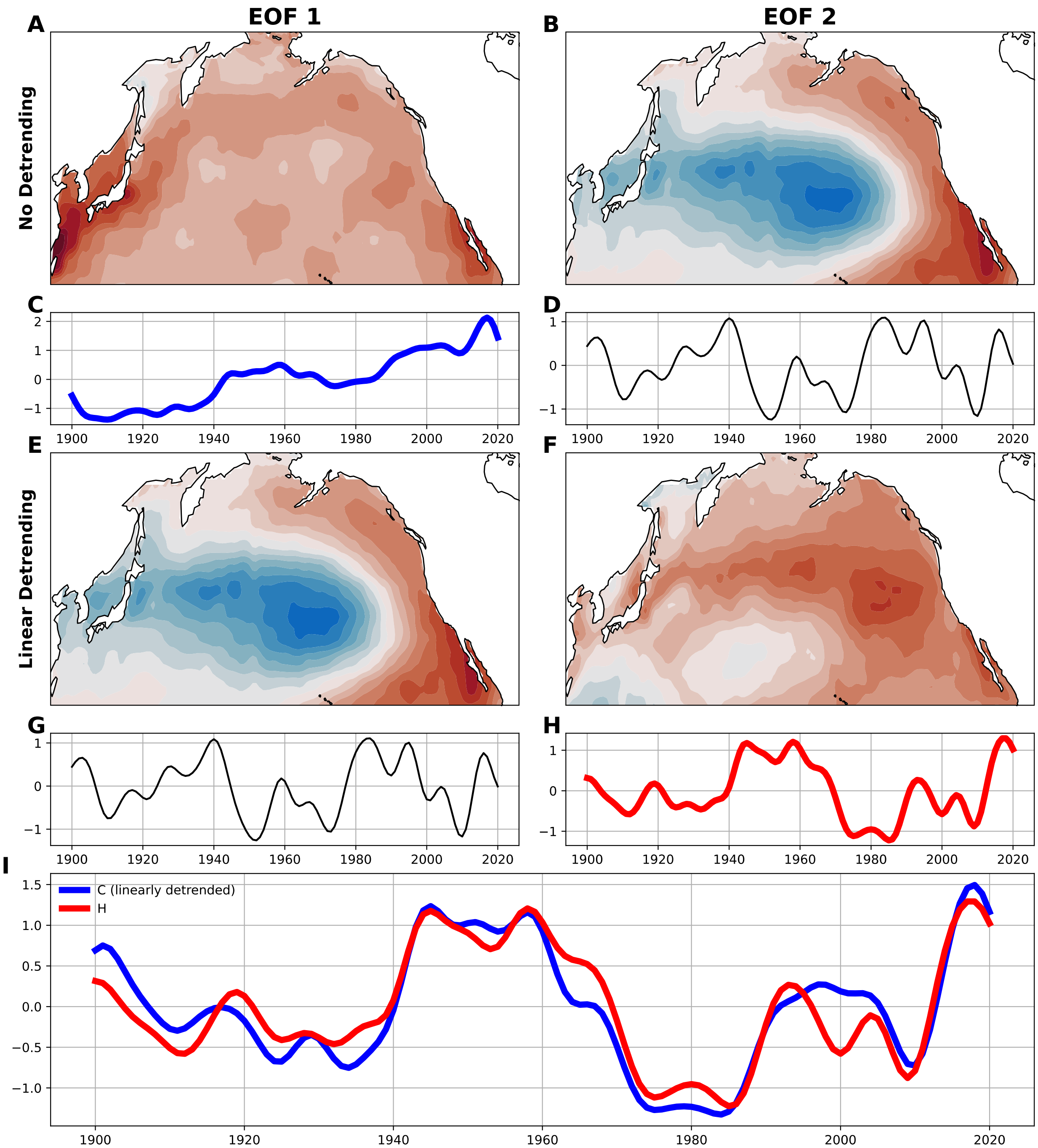

Figure 2. The effect linear detrending has on observed EOFs in the NP. For observations where no detrending occurs, A) and C) show the first EOF spatial pattern and time series respectively. B) and D) show the same but for the second EOF. For linearly detrended observations, E) and G) show the first EOF spatial pattern and time series respectively, while F) and H) show the same for the second EOF. I) shows the time series from C) (linearly detrended) and H) together to show their similarity (93% correlation, significant at the 99% threshold). The red curves are the same time series, while the blue curve in I) is equivalent to the time series in C) but with the linear slope removed.

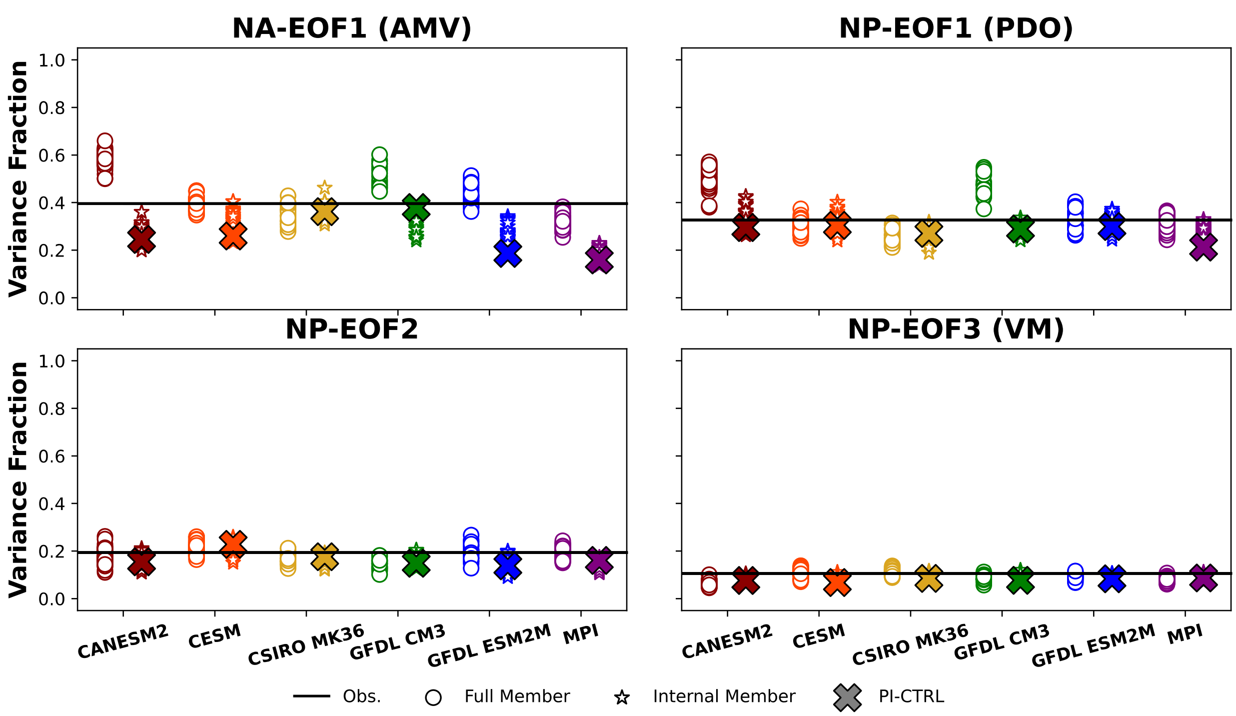

Figure 3. EOF variance explained of MMLEA ensemble members. Top row form left to right: NA-EOF1 and NP-EOF1. Bottom row form left to right: NP-EOF2 and NP-EOF3. Black lines represent observed values. Colors correspond to models as follows: dark red (CANESM2), orange (CESM), gold (CSIRO MK36), green (GFDL CM3), blue (GFDL ESM2M), and purple (MPI). For each model, two sub-columns are shown: the full, or total, variability on the left and the internal variability on the right. Each circle/star represents a single member. Xs represent pre-industrial control values.

Results: Model Assessment

Here, we want to assess how realistic the simulated modes are relative to the observed, including how much of the observed variability can be explained by forcing and internal variability. One way we can analyze this is to compare the fraction of explained variance for each EOF to the corresponding value for observations, as shown in Figure . EOF 1 in each basin shows some inter-model spread, but the observed value falls within the internal range for each model. For both basins, EOF 1 generally explains between 30-40% variance, while EOF 2 explains 15-20%, and EOF 3 around 10-15%. In some cases for each member, the full variability explains more variance than its corresponding internal variability. This can be attributed to the external forcing that is present in the full but not the internal. Generally, the internal variability should agree with the observations better than the full variability, although both appear relatively similar to the observed values. The MMLEA looks qualitatively similar enough to observations for this metric to proceed.

We also assess the realism of the MMLE subjectively by looking at the EOF spatial patterns. Supplemental Figure 2 shows the observed EOFs and the composite mean EOFs for each model. The MMLEA NA EOFs all roughly share a similar tripole spatial pattern to the observed first NA-EOF. The magnitude of the gradients across all ensembles differs from the observations, however. Extending from the Gulf Stream region, the MMLEA models generally show an opposite trend to the rest of the basin (cooling in the Gulf Stream region when the rest of the basin is warming), whereas the observations show uniform warming or cooling. In the NP, NP-EOF1 shows good agreement, all showing the classic PDO pattern. The second observed

EOF differs significantly from those in the MMLEA. The observed pattern shows uniform warming or cooling across the entire basin, while the third observed EOF shows a typical VM pattern. The MMLEA appears to skip over the uniform warming/cooling spatial pattern, showing only the PDO as EOF1 and the VM as EOF2 in most members. One possible explanation for this is that the observed EOF2 represents non-linear features of external forcing, which would successfully be removed in an MMLEA model by subtracting the ensemble mean, but not in observations through the linear detrending method. It is interesting that this is different in the Atlantic and Pacific, suggesting that method for removal of the forced signal is basin dependent. Generally, the MMLEA members do show internal modes similar to the observed modes (when comparing observed NP-EOF3 to MMLEA NP-EOF2), suggesting that the models simulate variability realistically enough to analyze potential mode interactions.

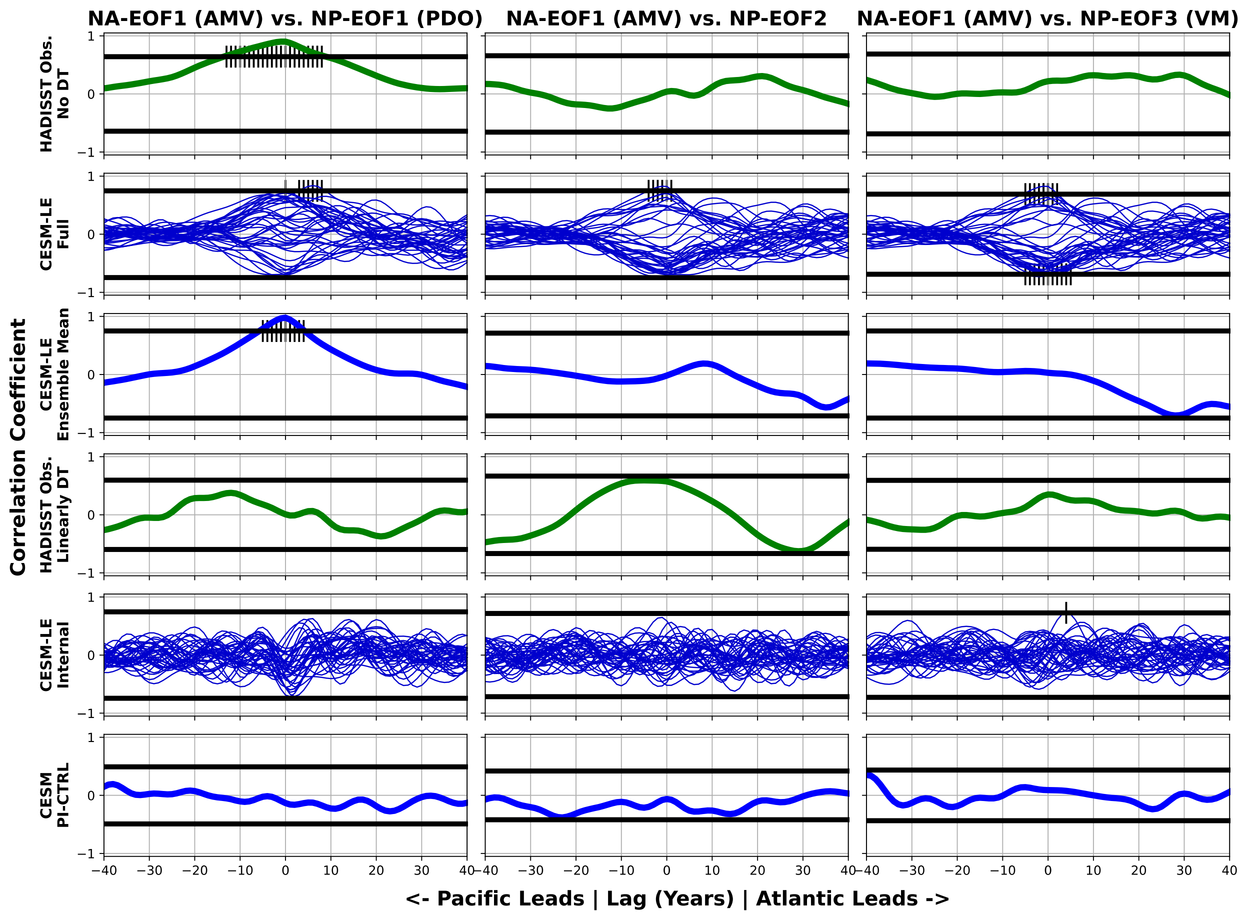

Figure 4. Cross-correlations of NA-NP mode relationships. From left to right: AMV (NA-EOF1) vs. PDO (NP-EOF1) relationship, AMV vs. NP-EOF2 relationship, and AMV vs. VM (NP-EOF3) relationship. From top to bottom: Observations with no detrending, CESM-LE (from MMLEA) full variability, CESM-LE ensemble mean, Observations with linear detrending, CESM-LE internal variability, and CESM pre-industrial control variability. Black horizontal lines are 95% statistical significance thresholds as calculated by the "peak" test. Vertical ticks show where cross-correlations are significant. For positive (negative) lags, the NA (NP) mode leads. All othe MMLEA large ensembles show qualitatively similar results.

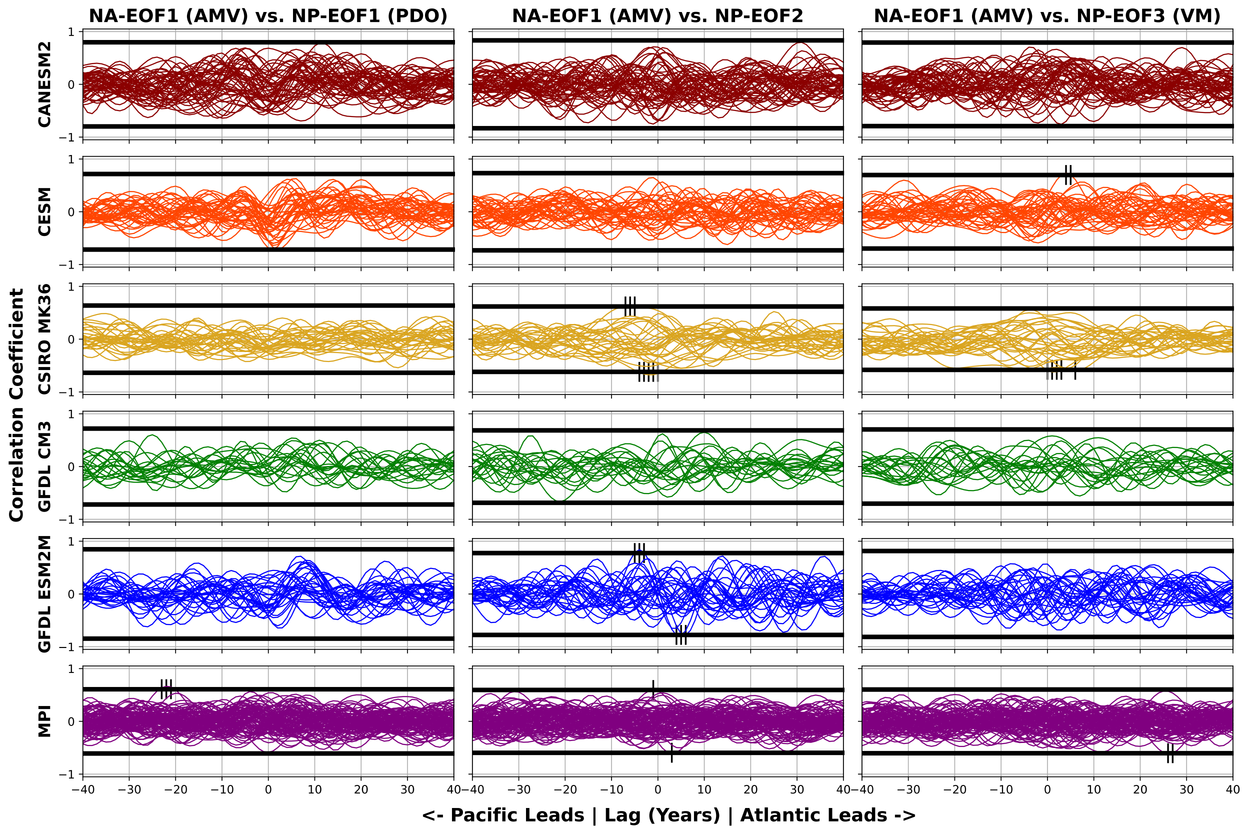

Figure 5. Cross-correlations of MMLEA internal only NA-NP mode relationships. From left to right: AMV (NA-EOF1) vs. PDO (NP-EOF1) relationship, AMV vs. NP-EOF 2, and AMV vs. VM. Black horizontal lines are 95% statistical significance thresholds as calculated by the "peak" test. Vertical ticks show where cross-correlations are significant. For positive (negative) lags, the NA (NP) mode leads. 269 MMLEA members are utilized for a total of 807 relationships. Only 11 (<2%) have statistically significant points.

Results: Relationship Analysis

Figure 4 shows a series of NA-NP relationships from observations and the CESM Large Ensemble (CESM-LE), one of the MMLEA ensembles. The top row shows the non-detrended (or full) observed EOF cross-correlations. Without detrending, the first EOF of each basin captures the global warming or externally forced signal. The signal in each basin is clearly connected, with significant points along a peak at 0 lag. This can be interpreted as global warming affecting each basin in a very similar way. The other relationships, which capture the internal modes in the NP, show no statistically significant connection.

The next row shows the relationships for full members of the CESM-LE. Again, most of these relationships show a peak near 0 lag for all three relationships. This suggests that external forcing affects all of the first three NP EOFs, such that a nearly significant peak appears near 0 lag for most members. When this global warming signal is shown by itself as the ensemble mean in the third row, the same connection as in the observed forced signals appears, with the forced signal in each basin being significantly correlated. Note that the ensemble mean EOFs 2 and 3 do not have a physical meaning and can be neglected. Also, averaging across all ensemble members may mutually cancel out polarized clusters of members, so caution must be used when computing ensemble means (Bellucci et al. 2017).

So far, we have shown that the combined internal and forced relationships are statistically significant, particularly only the forced relationships. Rows four through six analyze only the internal relationships to determine whether connections between the internal modes exist or not. Row four shows the linearly detrended observed relationships. The AMV-PDO relationship (hereafter all relationships referred to as AMV-PDO, AMV-VM, etc.) shows similar results as Wu et al. (2011), Marini and Frankignoul (2014), and Nigam et al. (2020), and both the AMV-PDO and AMV-NP-EOF2 show similar results as d'Orgeville and Peltier (2007) and Zhang and Delworth (2007). However, we show different significance thresholds as per the peak test. The sign of the correlation and the precise lag at which the maximum correlation occurs may slightly vary from study to study due to differing methods, particularly the sign of the EOF output and filter used. Linear detrending is also not ideal for removing the observed forced signal (Frankignoul et al. 2017), which may allow the forced signal to remain and cause a spurious higher correlation as seen in AMV-NP-EOF2.

To account for the inadequacy of linear detrending, the MMLEA internal relationships and the CESM PI are shown in rows five and six respectively. Only one of these 120 members show a significant relationship, suggesting that any internal connection between the NA and NP basins is indistinguishable from random noise. All other MMLEA ensembles show qualitatively similar results. Figure 5 shows the internal relationships for all six MMLEA ensembles analyzed, with only 11 out of 807 (<2%) relationships having any statistically significant points. The same concept of external forcing driving significant relationships appears in all of the ensembles, despite their various differences.

Discussion

Our results suggest that, for the NA and NP basins, an internal connection between the two does not need consideration as a potential source of variability. These findings may also have broader implications regarding the roles of external forcing and internal variability as drivers of climate modes. Present theories on climate mode drivers focus on varying roles for the ocean, atmosphere, internal variability, and external forcing (e.g. Clement et al. 2015, Newman et al. 2016, Wills et al. 2018, Zhang et al. 2018, O'Reilly et al. 2019, Zhang et al. 2019, etc.). External forcing is particularly challenging, due to the direct/linear and indirect/non-linear effects on climate variability (Frankignoul et al. 2017, Li et al. 2020). Additionally, there is debate about the role and importance of these internal modes in an increasingly forced global climate (Ting et al. 2009, DelSole et al. 2011, Haustein et al. 2019, Mann et al. 2020, etc.).

Additionally, our results suggest that traditional observed AMV and PDO definitions contain at least some external forcing. Care must be taken when using these mode definitions to properly remove the forced signal so as to isolate the internal variability. However, this is a challenging task outside of the realm of large ensembles. Tools such as the MMLEA will be vital in making progress toward isolating the forced response in observations, as they can possibly average out various model differences and provide a closer analog to the observed forced signal. These modeling tools are especially useful due to the relatively short observed period, which may not be sufficient to adequately observe variability on multi-decadal timescales, such as those studied here.

Finally, our findings do not rule out other regions or modes driving variability in the NA and NP. Other mode relationships have been shown to exist, such as how ENSO helps drive the

PDO (Newman et al. 2003). Further work can include a complex matrix of potential relationships between global modes as in Shin et al. (2010) or using global EOFs such as Nigam et al. (2020). Methods presented here can assist in a thorough decomposition of sources of variability in a particular region. This can lead to better understanding of variability drivers, which can ultimately result in improved climate models and more accurate climate forecasts.

Acknowledgments, Samples, and Data

The authors gratefully acknowledge funding from the NSF Climate and Large Scale Dynamics program and NOAA Climate Program Office that supported this work. We also acknowledge all modelling groups and the US CLIVAR Working Group on Large Ensembles for making their data available in the Multi-Model Large Ensemble data repository. We thank Brian Mapes and his Applied Data Analysis class for inspiration and discussions on proper statistical analysis.

Data Access: https://www.cesm.ucar.edu/projects/community-projects/MMLEA/ (MMLEA); https://www.metoffice.gov.uk/hadobs/hadisst/ (HADISST).

References

Alexander, M. A. (2002). The Atmospheric Bridge: The Influence of ENSO Teleconnections on Air–Sea Interaction over the Global Oceans. *JOURNAL OF CLIMATE*, *15*, 27.

An, X., Wu, B., Zhou, T., & Liu, B. (2021). Atlantic Multidecadal Oscillation Drives Interdecadal Pacific Variability via Tropical Atmospheric Bridge. *Journal of Climate*, *34*(13), 5543–5553. https://doi.org/10.1175/JCLI-D-20-0983.1

Bellucci, A., Mariotti, A., & Gualdi, S. (2017). The Role of Forcings in the Twentieth-Century North Atlantic Multidecadal Variability: The 1940–75 North Atlantic Cooling Case Study. *Journal of Climate*, *30*(18), 7317–7337. https://doi.org/10.1175/JCLI-D-16-0301.1

Bond, N. A., Overland, J. E., Spillane, M., & Stabeno, P. (2003). Recent shifts in the state of the North Pacific. *Geophysical Research Letters*, *30*(23). https://doi.org/10.1029/2003GL018597

Cane, M. A., Clement, A. C., Murphy, L. N., & Bellomo, K. (2017). Low-Pass Filtering, Heat Flux, and Atlantic Multidecadal Variability. *Journal of Climate*, *30*(18), 7529–7553. https://doi.org/10.1175/JCLI-D-16-0810.1

Clement, A., Bellomo, K., Murphy, L. N., Cane, M. A., Mauritsen, T., Radel, G., & Stevens, B. (2015). The Atlantic Multidecadal Oscillation without a role for ocean circulation. *Science*, *350*(6258), 320–324. https://doi.org/10.1126/science.aab3980

DelSole, T., Tippett, M. K., & Shukla, J. (2011). A Significant Component of Unforced Multidecadal Variability in the Recent Acceleration of Global Warming. *Journal of Climate*, *24*(3), 909–926. https://doi.org/10.1175/2010JCLI3659.1

Deser, C., Lehner, F., Rodgers, K. B., Ault, T., Delworth, T. L., DiNezio, P. N., et al. (2020). Insights from Earth system model initial-condition large ensembles and future prospects. *Nature Climate Change*. https://doi.org/10.1038/s41558-020-0731-2

Dommenget, D., & Latif, M. (2008). Generation of hyper climate modes. *Geophysical Research Letters*, *35*(2), L02706. https://doi.org/10.1029/2007GL031087

Eden, C., & Jung, T. (2001). North Atlantic Interdecadal Variability: Oceanic Response to the North Atlantic Oscillation (1865–1997). *JOURNAL OF CLIMATE*, *14*, 16.

Enfield, D. B., Mestas-Nuñez, A. M., & Trimble, P. J. (2001). The Atlantic Multidecadal Oscillation and its relation to rainfall and river flows in the continental U.S. *Geophysical Research Letters*, *28*(10), 2077–2080. https://doi.org/10.1029/2000GL012745

Frankignoul, C., Gastineau, G., & Kwon, Y.-O. (2017). Estimation of the SST Response to Anthropogenic and External Forcing and Its Impact on the Atlantic Multidecadal Oscillation and the Pacific Decadal Oscillation. *Journal of Climate*, *30*(24), 9871–9895. https://doi.org/10.1175/JCLI-D-17-0009.1

Ghasemi, A., & Zahediasl, S. (2012). Normality Tests for Statistical Analysis: A Guide for Non-Statisticians. *International Journal of Endocrinology and Metabolism*, *10*(2), 486–489. https://doi.org/10.5812/ijem.3505

Haustein, K., Otto, F. E. L., Venema, V., Jacobs, P., Cowtan, K., Hausfather, Z., et al. (2019). A Limited Role for Unforced Internal Variability in Twentieth-Century Warming. *Journal of Climate*, *32*(16), 4893–4917. https://doi.org/10.1175/JCLI-D-18-0555.1

Katz, R. W. (1982). Statistical Evaluation of Climate Experiments with General Circulation Models: A Parametric Time Seres Modeling Approach. *Journal of Atmospheric Sciences*, *39*(7), 1446-1455. https://ddoi.org/10.1175/1520-0469(1982)039<1446:SEOCEW>2.0CO;2

Kay, J. E., Deser, C., Phillips, A., Mai, A., Hannay, C., Strand, G., et al. (2015). The Community Earth System Model (CESM) Large Ensemble Project: A Community Resource for Studying Climate Change in the Presence of Internal Climate Variability. *Bulletin of the American Meteorological Society*, *96*(8), 1333–1349. https://doi.org/10.1175/BAMS-D-13-00255.1

Liu, Z., & Alexander, M. (2007). Atmospheric bridge, oceanic tunnel, and global climatic teleconnections. *Reviews of Geophysics*, *45*(2), RG2005. https://doi.org/10.1029/2005RG000172

Lorenzo, E. D., Schneider, N., Cobb, K. M., Franks, P. J. S., Chhak, K., Miller, A. J., et al. (2008). North Pacific Gyre Oscillation links ocean climate and ecosystem change. *Geophysical Research Letters*, *35*(8). https://doi.org/10.1029/2007GL032838

Mann, M. E., Steinman, B. A., & Miller, S. K. (2020). Absence of internal multidecadal and interdecadal oscillations in climate model simulations. *Nature Communications*, *11*(1), 49. https://doi.org/10.1038/s41467-019-13823-w

Mann, M. E., Steinman, B. A., Brouillette, D. J., & Miller, S. K. (2021). Multidecadal climate oscillations during the past millennium driven by volcanic forcing. *Science*, *371*(6533), 1014–1019. https://doi.org/10.1126/science.abc5810

Mantua, N. J., Hare, S. R., Zhang, Y., Wallace, J. M., & Francis, R. C. (1997). A Pacific Interdecadal Climate Oscillation with Impacts on Salmon Production*. *Bulletin of the American Meteorological Society*, *78*(6), 1069–1080. https://doi.org/10.1175/1520-0477(1997)078<1069:APICOW>2.0.CO;2

Maraun, D. (2013). Bias Correction, Quantile Mapping, and Downscaling: Revisiting the Inflation Issue. *Journal of Climate*, *26*(6), 2137–2143. https://doi.org/10.1175/JCLI-D-12-00821.1

Marini, C., & Frankignoul, C. (2014). An attempt to deconstruct the Atlantic Multidecadal Oscillation. *Climate Dynamics*, *43*(3), 607–625. https://doi.org/10.1007/s00382-013-1852-3

Martin, T., Reintges, A., & Latif, M. (2019). Coupled North Atlantic Subdecadal Variability in CMIP5 Models. *Journal of Geophysical Research: Oceans*, *124*(4), 2404–2417. https://doi.org/10.1029/2018JC014539

Newman, M., Compo, G. P., & Alexander, M. A. (2003). ENSO-Forced Variability of the Pacific Decadal Oscillation. *JOURNAL OF CLIMATE*, *16*, 5.

Newman, M., Alexander, M. A., Ault, T. R., Cobb, K. M., Deser, C., Di Lorenzo, E., et al. (2016). The Pacific Decadal Oscillation, Revisited. *Journal of Climate*, *29*(12), 4399–4427. https://doi.org/10.1175/JCLI-D-15-0508.1

Nigam, S., Sengupta, A., & Ruiz-Barradas, A. (2020). Atlantic–Pacific Links in Observed Multidecadal SST Variability: Is the Atlantic Multidecadal Oscillation's Phase Reversal Orchestrated by the Pacific Decadal Oscillation? *Journal of Climate*, *33*(13), 5479–5505. https://doi.org/10.1175/JCLI-D-19-0880.1

O'Reilly, C. H., Zanna, L., & Woollings, T. (2019). Assessing External and Internal Sources of Atlantic Multidecadal Variability Using Models, Proxy Data, and Early Instrumental Indices. *Journal of Climate*, *32*(22), 7727–7745. https://doi.org/10.1175/JCLI-D-19-0177.1

d'Orgeville, M., & Peltier, W. R. (2007). On the Pacific Decadal Oscillation and the Atlantic Multidecadal Oscillation: Might they be related?: PDO AND AMO RELATED? *Geophysical Research Letters*, *34*(23), n/a-n/a. https://doi.org/10.1029/2007GL031584

Qin, M., Dai, A., & Hua, W. (2020). Quantifying contributions of internal variability and external forcing to Atlantic multidecadal variability since 1870. *Geophysical Research Letters*. https://doi.org/10.1029/2020GL089504

Raible, C. C., Lehner, F., González-Rouco, J. F., & Fernández-Donado, L. (2014). Changing correlation structures of the Northern Hemisphere atmospheric circulation from 1000 to 2100 AD. *Climate of the Past*, *10*(2), 537–550. https://doi.org/10.5194/cp-10-537-2014

Rayner, N. A. (2003). Global analyses of sea surface temperature, sea ice, and night marine air temperature since the late nineteenth century. *Journal of Geophysical Research*, *108*(D14), 4407. https://doi.org/10.1029/2002JD002670

Salinger, M. J., Renwick, J. A., & Mullan, A. B. (2001). Interdecadal Pacific Oscillation and South Pacific climate. *International Journal of Climatology*, *21*(14), 1705–1721. https://doi.org/10.1002/joc.691

Shin, S.-I., Sardeshmukh, P. D., & Pegion, K. (2010). Realism of local and remote feedbacks on tropical sea surface temperatures in climate models. *Journal of Geophysical Research*, *115*(D21), D21110. https://doi.org/10.1029/2010JD013927

Ting, M., Kushnir, Y., Seager, R., & Li, C. (2009). Forced and Internal Twentieth-Century SST Trends in the North Atlantic. *Journal of Climate*, *22*(6), 1469–1481. https://doi.org/10.1175/2008JCLI2561.1

Wills, R. C., Schneider, T., Wallace, J. M., Battisti, D. S., & Hartmann, D. L. (2018). Disentangling Global Warming, Multidecadal Variability, and El Niño in Pacific Temperatures. *Geophysical Research Letters*, *45*(5), 2487–2496. https://doi.org/10.1002/2017GL076327

Wills, R. C. J., Armour, K. C., Battisti, D. S., & Hartmann, D. L. (2019). Ocean–Atmosphere Dynamical Coupling Fundamental to the Atlantic Multidecadal Oscillation. *Journal of Climate*, *32*(1), 251–272. https://doi.org/10.1175/JCLI-D-18-0269.1

Wu, S., Liu, Z., Zhang, R., & Delworth, T. L. (2011). On the observed relationship between the Pacific Decadal Oscillation and the Atlantic Multi-decadal Oscillation. *Journal of Oceanography*, *67*(1), 27–35. https://doi.org/10.1007/s10872-011-0003-x

Yap, B. W., & Sim, C. H. (2011). Comparisons of various types of normality tests. *Journal of Statistical Computation and Simulation*, *81*(12), 2141–2155. https://doi.org/10.1080/00949655.2010.520163

Zhang, R., & Delworth, T. L. (2007). Impact of the Atlantic Multidecadal Oscillation on North Pacific climate variability: IMPACT ON NORTH PACIFIC VARIABILITY. *Geophysical Research Letters*, *34*(23), n/a-n/a. https://doi.org/10.1029/2007GL031601

Zhang, R., Sutton, R., Danabasoglu, G., Kwon, Y., Marsh, R., Yeager, S. G., et al. (2019). A Review of the Role of the Atlantic Meridional Overturning Circulation in Atlantic Multidecadal Variability and Associated Climate Impacts. *Reviews of Geophysics*, 2019RG000644. https://doi.org/10.1029/2019RG000644

Zhang, Y., Xie, S.-P., Kosaka, Y., & Yang, J.-C. (2018). Pacific Decadal Oscillation: Tropical Pacific Forcing versus Internal Variability. *Journal of Climate*, *31*(20), 8265–8279. https://doi.org/10.1175/JCLI-D-18-0164.1